JGP Journal of General Physiology

RESEARCH ARTICLE

Calcium-dependent inactivation controls cardiac L-type Ca^{2+} currents under β-adrenergic stimulation

Danna Morales[1], Tamara Hermosilla[2], and Diego Varela[1,2]

The activity of L-type calcium channels is associated with the duration of the plateau phase of the cardiac action potential (AP) and it is controlled by voltage- and calcium-dependent inactivation (VDI and CDI, respectively). During β-adrenergic stimulation, an increase in the L-type current and parallel changes in VDI and CDI are observed during square pulses stimulation; however, how these modifications impact calcium currents during an AP remains controversial. Here, we examined the role of both inactivation processes on the L-type calcium current activity in newborn rat cardiomyocytes in control conditions and after stimulation with the β-adrenergic agonist isoproterenol. Our approach combines a self-AP clamp (sAP-Clamp) with the independent inhibition of VDI or CDI (by overexpressing $Ca_V\beta_{2a}$ or calmodulin mutants, respectively) to directly record the L-type calcium current during the cardiac AP. We find that at room temperature (20–23°C) and in the absence of β-adrenergic stimulation, the L-type current recapitulates the AP kinetics. Furthermore, under our experimental setting, the activity of the sodium–calcium exchanger (NCX) does not affect the shape of the AP. We find that hindering either VDI or CDI prolongs the L-type current and the AP in parallel, suggesting that both inactivation processes modulate the L-type current during the AP. In the presence of isoproterenol, wild-type and VDI-inhibited cardiomyocytes display mismatched L-type calcium current with respect to their AP. In contrast, CDI-impaired cells maintain L-type current with kinetics similar to its AP, demonstrating that calcium-dependent inactivation governs L-type current kinetics during β-adrenergic stimulation.

Introduction

L-type calcium channels (LTCCs) represent the main Ca^{2+}-influx pathway involved in excitation–contraction coupling in cardiac muscle (Benitah et al., 2010). Ca^{2+} influx through LTCCs promotes the opening of ryanodine receptors and the subsequent Ca^{2+} release from the sarcoplasmic reticulum that establishes the rate and magnitude for cardiac muscle contraction in a process called calcium-induced calcium release (Fabiato, 1983). Many of the proteins involved in calcium-induced calcium release are regulated in the "fight or flight" response, a conserved sympathetic stress reaction leading to accelerated heart rate and increased contraction force of the heart (Marks, 2013). The cardiac response to sympathetic activation largely depends on β-adrenergic receptor (β-AR) activation and PKA-mediated phosphorylation of key residues (Woo and Xiao, 2012).

Although the auxiliary subunit $Ca_V\beta$ (Haase et al., 1996; Bünemann et al., 1999) and the pore-forming subunit $Ca_V1.2$ (Hulme et al., 2006; Fuller et al., 2010) of the LTCC can be phosphorylated by PKA, only $Ca_V1.2$ phosphorylation has been proposed as relevant for β-adrenergic regulation (Miriyala et al., 2008; Weiss et al., 2013; but see Katchman et al., 2017). Functionally, β-adrenergic stimulation causes an approximately threefold surge in LTCC activity in cardiomyocytes as a result of an increase in channel open probability (P_O). The latter occurs by a change in Ca^{2+} channel gating mode from an inactive mode, combined with a low P_O mode, to a gating mode characterized by high P_O with clusters of long and frequent openings (Tsien et al., 1986; Yue et al., 1990). At the whole-cell level, the macroscopic L-type calcium current amplitude increases, voltage dependence of activation shifts to more negative potentials, and the inactivation rates accelerate (Tsien et al., 1986; Findlay, 2004).

L-type current inactivates via two distinct mechanisms: a voltage-dependent (VDI) that is regulated by $Ca_V\beta$ and a calcium-dependent (CDI) regulated by calmodulin (CaM; Peterson et al., 1999). Both processes are thought to limit the amount of calcium influx during the action potential (AP). However, to what extent each inactivation process limits L-type current function during an AP is unclear. It is generally accepted that CDI predominates under physiological conditions (Grandi et al., 2010). Nevertheless, other studies show VDI predominance at positive membrane potentials, when calcium influx is

[1]Millennium Nucleus of Ion Channels-Associated Diseases (MiNICAD), Universidad de Chile, Santiago, Chile; [2]Programa de Fisiología y Biofísica, Instituto de Ciencias Biomédicas, Facultad de Medicina, Universidad de Chile, Santiago, Chile.

Correspondence to Diego Varela: dvarela@uchile.cl.

limited by electrochemical equilibrium (Findlay, 2004). Upon β-adrenergic stimulation, CDI has been suggested to dominate L-type current kinetics as a result of an incremented calcium influx and slower VDI (Kumari et al., 2018); however, the experimental data in this area are scarce and controversial (Morotti et al., 2012).

In this work, we use molecular tools to dissect the effect of independently reducing VDI or CDI on L-type calcium current kinetics during the ventricular APs in newborn rat cardiomyocytes in control conditions and upon isoproterenol stimulation. For that, we overexpressed the $Ca_V\beta_{2a}$ subunit, known to dramatically slow down VDI, and made use of a mutant version of calmodulin (CaM_{34}), known to abolish CDI. Under these conditions, we recorded nifedipine-sensitive currents with the self-AP clamp (sAP-Clamp) configuration in control and isoproterenol-treated cardiomyocytes. We show that both inactivation processes are important in the regulation of the L-type calcium current during the AP of control cardiomyocytes. Furthermore, L-type current inactivation is accelerated upon isoproterenol treatment and when the $Ca_V\beta_{2a}$ subunit is overexpressed, but not when the CaM_{34} mutant is expressed, thereby demonstrating that in cardiomyocytes under β-adrenergic stimulation, CDI (and not VDI) is responsible for L-type current regulation during the AP.

Materials and methods

Primary culture of neonatal rat cardiomyocytes

Rats were bred in the Animal Breeding Facility of the Facultad de Medicina, Universidad de Chile (Santiago, Chile). All studies were done in accordance and with the approval of the Institutional Bioethical Committee of Universidad de Chile. Cardiomyocytes were isolated enzymatically from neonatal Sprague-Dawley rats (P0-1), as previously described (Hermosilla et al., 2011; Moreno et al., 2015). Briefly, immediately after euthanasia, hearts were removed and minced in Hanks' solution (in mM): 116 NaCl, 5.4 KCl, 0.8 NaH_2PO_4, 0.8 $MgSO_4$, 5.6 glucose, 20 HEPES (pH 7.4, adjusted with NaOH). The tissue was then digested with pancreatin (1.2 mg/ml; Sigma) and collagenase type II (0.2 mg/ml; Invitrogen) for 15 min at 37°C under constant agitation. Thereafter, the supernatant was discarded and replaced with fresh digestion solution (15 min at 37°C, by agitation). Cells were spun (5 min at 900 x*g*), the supernatant discarded, and the cells resuspended in 1.5 ml of horse serum. This was repeated five times and the collected cells were resuspended in Dulbecco's modified Eagle's medium (DMEM; Invitrogen) supplemented with 15% horse serum and 1% antibiotic (Pen/Strept). The cell suspension was plated in a culture dish and incubated for 2 h (37°C, 95% O_2: 5% CO_2) to allow fibroblast adhesion. Nonadherent cells (cardiomyocytes) were recovered from the supernatant and centrifuged (5 min at 900 x*g*) and seeded onto gelatin (1%)-coated culture plates. Sixteen hours later, the medium was replaced with DMEM 0.5% FBS.

Cardiomyocyte infection

The number of viral particles for each adenovirus was determined by 260-nm absorbance and was in the order of 10^{11} particles per milliliter. The effective virus titer was determined at 90% infection efficiency by RFP fluorescence in the absence of cytopathic effects. Infection was performed at seeding on gelatin-coated plates with 10^9 particles of the $Ca_V\beta_{2a}$ adenoviral construct per dish. After 16 h, the medium was replaced with DMEM media supplemented with 0.5% FBS. Cells were used 48 h after infection.

Cardiomyocyte transfection

Neonatal cardiomyocyte transfection was used to induce the expression of CaM_{WT} and CaM_{34} (kindly provided by Dr. Ivy Dick). Transfection of CaM complementary DNA was performed with Lipofectamine LTX (Invitrogen) according to the manufacturer's protocol, using 1 µg DNA/dish in serum-free medium for 6 h. The transfected cells were used 48–72 h after transfection. Effective transfection was assessed by GFP fluorescence.

Electrophysiological recordings

Membrane potential and membrane currents were recorded at room temperature (20–23°C) or at physiological temperature (35–37°C) using the patch-clamp technique in whole-cell recording mode (Hamill et al., 1981). Temperature was controlled with a TC-344C heater controller (Warner Instruments). Borosilicate glass pipettes (World Precision Instruments) were pulled to have 2–4-MΩ resistance using a P70 horizontal puller (Sutter Instruments) and filled with internal solution containing (in mM) the following: 120 KCl, 1.5 $MgCl_2$, 10 HEPES, 0.5 EGTA, 0.01 $CaCl_2$, 5 MgATP, and 0.6 LiGTP (pH 7.2 adjusted with KOH); the bath solution contained 140 NaCl, 4 KCl, 2 $CaCl_2$, 1 $MgCl_2$, 10 HEPES, and 10 glucose (pH 7.4 adjusted with NaOH). Membrane potentials were sampled at 10 kHz using a 1322a Digidata (Axon Instruments). Cell capacitance, series resistance (compensation, 70–80%), and junction potentials were compensated using the circuitry of the AxoPatch 200B amplifier (Molecular Devices) and low-pass filtered at 5 kHz. sAP-Clamp protocols, data acquisition, storage, analysis, current fitting, and offline subtraction were performed using Clampfit 9.2 (Molecular Devices); and all curves were fitted with SigmaPlot 11 (Systat Software, Inc.).

sAP-Clamp

To perform sAP-Clamp, the AP of the cardiomyocyte was first recorded (Hermosilla et al., 2017) under the current-clamp mode. APs were elicited by depolarizing current injections through the patch electrode (stimulation frequency, 1–5 Hz). Membrane currents were elicited on the same cells in which the AP waveform was recorded by digitizing the average of >20 APs previously recorded. Stimulation frequency was the same as that of the AP acquisition frequency. Cells displaying nonzero baseline or with rundown were discarded. K_{Ca}-currents were recorded by inhibition with a cocktail of apamin (100 nM), iberiotoxin (5 nM), and TRAM34 (100 nM) added to the bath. The ionic current carried by L-type channels was isolated offline by subtracting currents after application of a saturating concentration of nifedipine (10 µM). The holding potential between the voltage pulses was always −80 mV. Isoproterenol (100 nM) was used to study the effect of β-adrenergic action on LTCCs.

Data analysis

AP duration (APD) was determined at 20%, 50%, 90%, and 100% of repolarization (APD_{20}, APD_{50}, APD_{90}, and APD, respectively) measuring the average AP of at least 20 consecutive APs. For each condition, phase plots were constructed by plotting the temporal derivative of averaged APs (dV/dt), determined against the instantaneous membrane potential value (V). Diastolic membrane potential (DMP), threshold potential (defined as the point where dV/dt exceeds 10% of its maximum value), overshoot (voltage value where the first derivate is equal to zero), and the maximum upstroke velocity (dV/dt_{max}) were obtained from these phase plots. The current density (pA/pF) was estimated by measuring the amplitude of the current and dividing it by the cellular capacitance (Cm). The total time of the current (TTC) was measured manually and normalized with respect to the duration of its own AP (TTC_{norm}), while the time that the current takes to reach the peak (TTP) was used as readout of the activation kinetics. Finally, the charge carried by the L-type current was calculated by integrating the current traces and normalizing by Cm.

Mathematical model

The inactivation contribution to the L-type currents in Fig. 3 and the L-type currents displayed in Fig. 7 were simulated using MATLAB R2017a (Mathworks) based on previously published models. The model assumes 15 ionic currents, 6 intracellular Ca^{2+} fluxes, and 37 state variables (Wang and Sobie, 2008). The time-dependent changes in membrane potential is computed by solving the ordinary differential equation

$$\frac{dV}{dt} = -\frac{1}{C_m}(I_{Na} + I_{Na_b} + I_{Ca_L} + I_{Ca_T} + I_{Ca_b} + I_{p_{Ca}} + I_{NCX} + I_{NaK} + I_{K_{tof}} + I_{K_{ur}} + I_{K_r} + I_{K_s} + I_{K_{ss}} + I_{K_1} + I_{Cl_{Ca}}), \quad (1)$$

where Cm is the normalized membrane capacitance assumed to be 1 μF/cm². Model currents included I_{Na}, Na^+ current; I_{Nab}, background Na^+ current; I_{NaK}, Na-K pump current; I_{Ktof}, fast transient outward K^+ current; I_{Ks}, slow delayed rectifier K^+ current; I_{Kr}, rapid delayed rectifier K^+ current; I_{Kur}, ultrarapid delayed rectifier K^+ current; I_{Kss}, steady-state K^+ current; I_{K1}, inward rectifier K^+ current; $I_{Cl,Ca}$, Ca^{2+}-activated Cl^- current; I_{CaT}, T-type Ca^{2+} current; I_{CaB}, background Ca^{2+} current; I_{PCa}, Ca^{2+} pump current; I_{NCX}, Na/Ca exchanger current.

The L-type current assumes four closed states, three inactivation states, and one open state as depicted in Fig. 3 and described in (Bondarenko et al., 2004; Wang and Sobie, 2008).

Statistics

All values are reported as mean ± SEM. Statistical analyses of the data were performed with SigmaPlot 11 (Systat Software, Inc.) using the unpaired Student's *t* test when two groups were compared or one-way ANOVA if more than two groups were compared; in both cases, the significance was considered at $P < 0.05$.

Online supplemental material

Fig. S1 shows APs recorded with high extracellular calcium. Fig. S2 shows APs recorded at different acquisition frequencies. Fig. S3 shows calcium-activated potassium currents during the AP in control and isoproterenol-stimulated cardiomyocytes. Fig. S4 shows the role of sodium–calcium exchanger (NCX) in shaping the AP at 21–23°C. Fig. S5 shows the complementary role of VDI and CDI on APs.

Results

β-Adrenergic stimulation modifies APs in different ways depending on the species (Kääb et al., 1996; Song et al., 2001; O'Hara and Rudy, 2012; Xu et al., 2016) and therefore our first aim was to describe the effect of isoproterenol on the AP of newborn rat cardiomyocytes. Fig. 1 A shows typical newborn rat cardiomyocyte APs, evoked at 1 Hz, before and after isoproterenol (100 nM) treatment. To further examine the elicited APs, phase-plane plots were generated by graphing the voltage derivative in time (dV/dt) versus voltage (Fig. 1 B). Given the slow repolarization kinetics compared with that of the depolarization phase, these graphs mainly illustrate the initial part of the AP, where the voltage derivate is positive. Thus, they evidence important parameters to consider during AP analysis (see Materials and methods), such as the threshold potential, maximum upstroke velocity (dV/dt_{max}), maximal depolarization voltage (overshoot), and DMP. Isoproterenol treatment does not produce significant alterations to any of these parameters (Fig. 1, C and D), whereas quantification of the repolarization phase highlights significant differences at every APD determined (APD_{20}, APD_{50}, and APD_{90}) in isoproterenol-treated cardiomyocytes (Fig. 1 E), indicating that isoproterenol increases potassium and/or diminishes calcium currents in these cells.

To evaluate if the size of the calcium currents was involved in the observed APD differences, we studied the effect of incrementing the calcium current on the APs by recording APs from cardiomyocytes with 5 mM Ca^{2+} in the bath solution (Fig. S1) or from cardiomyocytes stimulated at 3 and 5 Hz to promote L-type facilitation (Fig. S2). Under these conditions, only the AP overshoot, threshold, and dV/dt_{max} at different stimulation frequencies differed when compared with those recorded in control cells (Figs. S1 and S2). In contrast to our observations in isoproterenol-stimulated cardiomyocytes, the repolarization phase was unaltered by neither treatment, demonstrating that an increase in the L-type Ca^{2+} current is not sufficient to modify APD in newborn rat cardiomyocytes.

To directly record the L-type Ca^{2+} current during the AP, we used the sAP-Clamp configuration (see Materials and methods); 10 μM nifedipine was used to inhibit L-type currents, a concentration that abrogates 96.6 ± 0.3% ($n = 6$) of the Ca^{2+} current. Diminishing calcium influx prevents calcium-dependent potassium current activation, and thus the magnitude of K_{Ca} currents (IK_{Ca}) was evaluated in control and in isoproterenol-stimulated cardiomyocytes (Fig. S3). Under our experimental setting, small, isoproterenol-insensitive IK_{Ca} was detected, and therefore we surmise that the nifedipine-sensitive current measured corresponds to L-type Ca^{2+} current.

When the nifedipine-sensitive current was studied, it showed kinetics similar to those of the AP itself (Fig. S3), an observation reinforced by the fact that, given the very positive

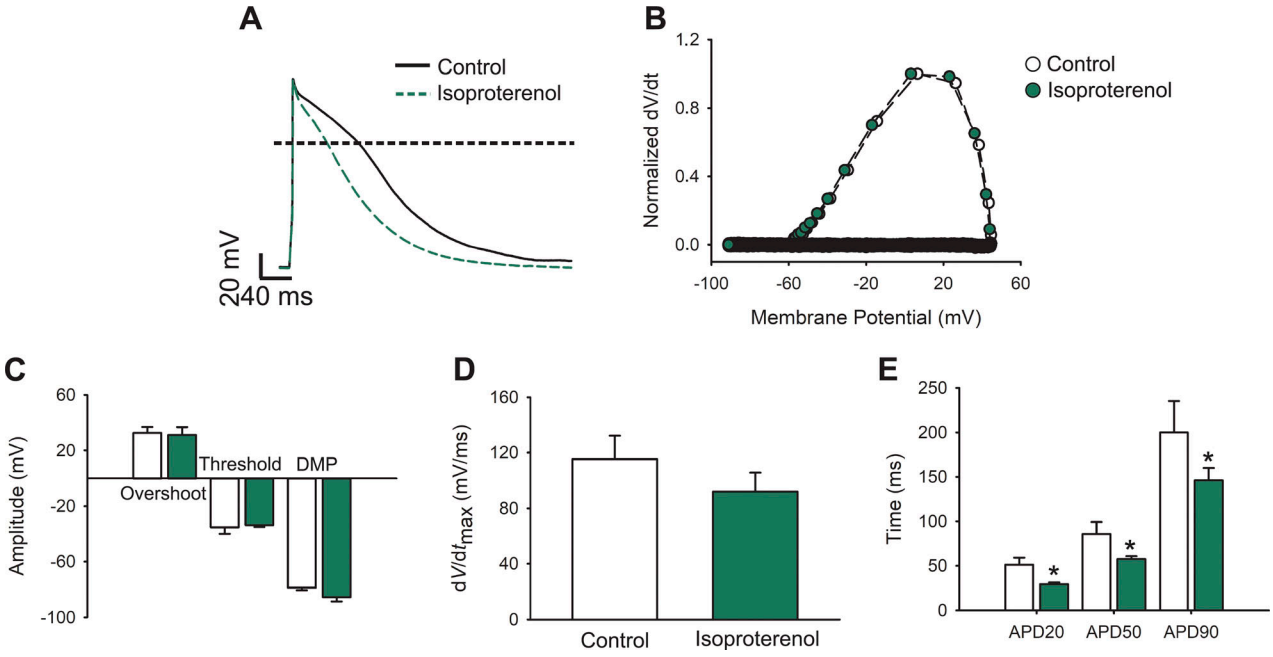

Figure 1. **APs from isoproterenol-treated cardiomyocytes. (A)** Representative AP waveforms from a cardiomyocyte before (black solid line) and after (green dashed line) 100 nM isoproterenol application. APs were elicited by 2–5 ms depolarizing current injections (100–200 pA) at 1 Hz. The horizontal line indicates zero level. **(B)** Phase plot of the normalized first derivative of membrane potential (dV/dt) against membrane potential (V_m) for the APs shown in A. **(C)** Bar graph of overshoot, threshold potentials, and mean DMPs. **(D)** Bar graph of maximum rate of potential change (dV/dt_{max}). **(E)** Bar graphs of APD estimated at 20%, 50%, and 90% of the repolarization phase (APD_{20}, APD_{50}, and APD_{90}, respectively). Bar graphs are mean ± SEM; empty bars are control cardiomyocytes, and green bars correspond to isoproterenol-treated cardiomyocytes (n = 10; *P < 0.01, with respect to control).

calcium equilibrium potential (E_{Ca}), the driving force for calcium current is mainly dependent on the membrane potential. To evaluate this preliminary finding, both responses were normalized (to maximum absolute value) and plotted together with the nifedipine-sensitive current inverted just for display purposes (Fig. 2 A).

With the aim to extrapolate our results to other species, we used a mathematical model that describes the ionic currents and Ca^{2+} transport mechanisms in the neonatal mouse cardiomyocyte (Wang and Sobie, 2008). This model could not recapitulate the match between the kinetics of the L-type current and the AP, as shown in Fig. 3. As the repolarization phase of the AP is the result of the concerted activation of many ion channels, exchangers, and pumps, the reason for this discrepancy between our data and the model could be attributed to multiple factors; however, because NCX activity has been involved in the plateau phase of the AP in other species (Armoundas et al., 2003; Ramos-Franco et al., 2016), we explored the role of this exchanger in the AP of cardiomyocytes from newborn rats.

To accomplish this, APs and nifedipine-sensitive currents were recorded from cardiomyocytes treated with the NCX inhibitor SEA0400 (Tocris, 1 µM). No differences were detected in APD or any other evaluated parameter (Fig. S4). Moreover, nifedipine-sensitive current kinetics remained similar to the AP form (Fig. S4), as was seen under the control condition (Fig. 2 A).

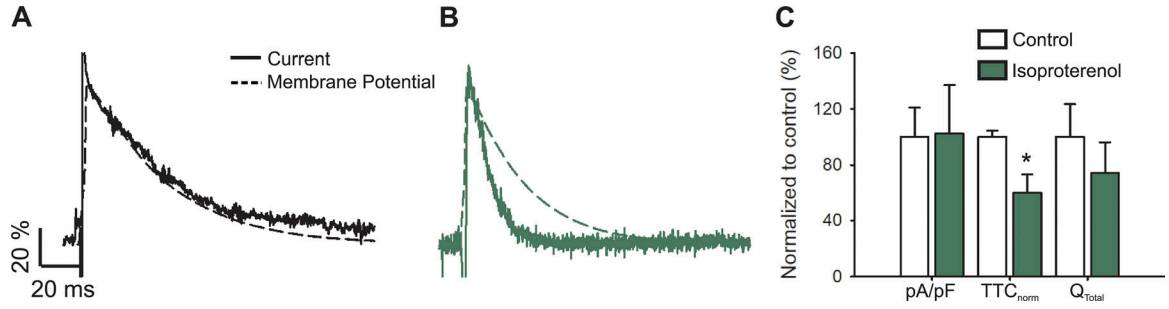

Figure 2. **L-type calcium current during an AP upon β-adrenergic stimulus. (A and B)** Representative nifedipine-sensitive current (solid line) elicited by the AP (dashed line) prerecorded from the same cell in control (A) and isoproterenol-treated (B) newborn rat cardiomyocytes. **(C)** Bar graph of maximal current normalized by cell capacitance (pA/pF); total time of nifedipine-sensitive current normalized by its APD (TTC_{norm}); and the total current integral normalized by cell capacitance (Q_{total}). Data are presented as percentages with respect to the controls. The bar graph shows mean ± SEM; empty bars represent control cardiomyocytes and green bars correspond to isoproterenol-treated cardiomyocytes (n = 6; *P < 0.01 with respect to control).

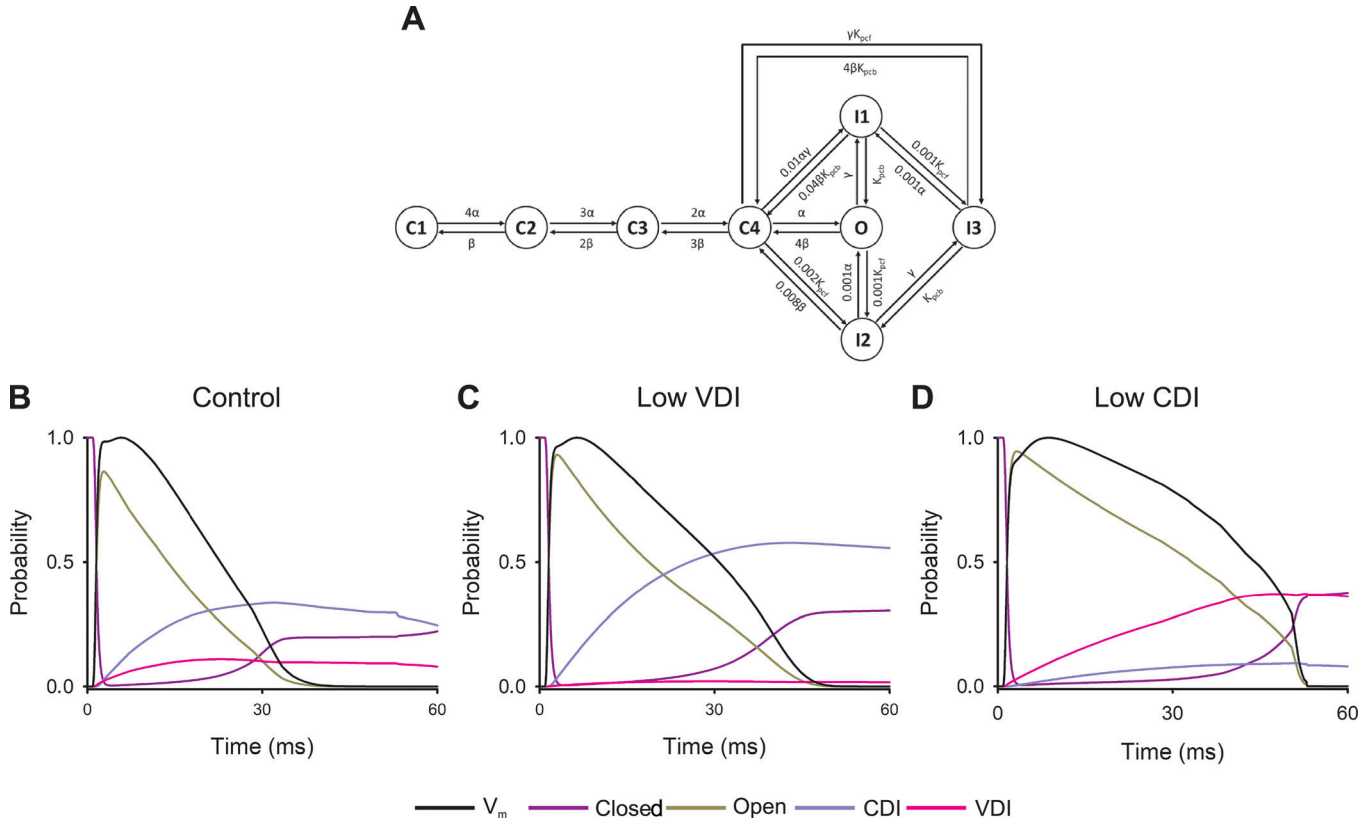

Figure 3. **L-type channel inactivation processes during the AP. (A)** State diagram of the model for L-type Ca^{2+} channel, the model assumes four closed states (C1, C2, C3, C4), three inactivation states (I1, I2, I3), and one open state (O). Voltage-dependent constants are α and β while γγ is calcium dependent. K_{pcf} and K_{pcb} are voltage-insensitive rate constants. **(B–D)** Probability of open (dark yellow line), closed (violet line), CDI (light purple line), or VDI (pink line) states of LTCCs during a simulated AP simulated in control cardiomyocytes (A) or with reduced VDI (B) or CDI (C). Normalized membrane potential (V_m, black line) for each scenario is shown for comparison.

To further explore the role of NCX, we enhanced its activity by performing experiments at 35–37°C and show that, at this temperature range, APs are not only shorter than those at 20–23°C (Fig. 4, A and C) but the velocity of the nifedipine-sensitive current kinetics is more pronounced than the AP, evidencing a mismatch between their kinetics (Fig. 4, D and F). Importantly, NCX inhibition at physiological temperatures further decreases the repolarization phase of the AP (Fig. 4, B and C), restoring the match between the nifedipine-sensitive current and the AP kinetics (Fig. 4, E and F). These experiments indicate that NCX is not involved in maintaining the plateau phase of APs in cardiomyocytes from newborn rats under our control experimental setting, which may explain the inadequacy of this model to describe our observations presented in this report.

Nevertheless, the mouse cardiomyocyte mathematical model allows predictions about the behavior of each individual inactivation process during the AP. As concluded previously (Findlay, 2004; Morotti et al., 2012; Kumari et al., 2018), both inactivation processes define the L-type current kinetics during the AP (Fig. 3 B), and thus a decrease in either inactivation would induce AP prolongation (Fig. 3, C and D). Importantly, the model also implies that the transition to the closed states per se defines the last part of the AP when either VDI or CDI is impaired (Fig. 3, B–D).

In view of these predictions, we performed experiments to demonstrate the relevance of each inactivation process in the control of L-type calcium current during the AP. CDI was abolished by overexpressing a mutant version of CaM where two aspartates from the C-terminal lobe are mutated to alanine (CaM_{34}), rendering the high-calcium-affinity lobe insensitive to Ca^{2+} (Peterson et al., 1999). Control experiments were performed in cells transfected with wild-type CaM. In agreement with Alseikhan et al. (2002), expression of CaM_{34} prolonged the APD when compared with cardiomyocytes transfected with CaM_{wt} (476 ± 120 versus 130 ± 12 ms; Fig. 5 A); changes in DMP were also observed. Other parameters such as overshoot, threshold voltage (Fig. 5, C and D), or dV/dt_{max} (66.4 ± 15.2 and 61.5 ± 10.8 V/ms, respectively) were unaltered.

Remarkably, although APD in CaM_{34}-overexpressing cardiomyocytes was almost four times longer than that of CaM_{wt}-overexpressing cardiomyocytes (Fig. 5 B), the nifedipine-sensitive current prolonged its duration accordingly (Fig. 5 E). To account for cell-to-cell current and APD variability, current durations were normalizing by dividing their total activated time by the duration of the AP recorded on the same cell (TTC_{norm}). In this way, deviations from 1 indicate mismatches between the current and the APD.

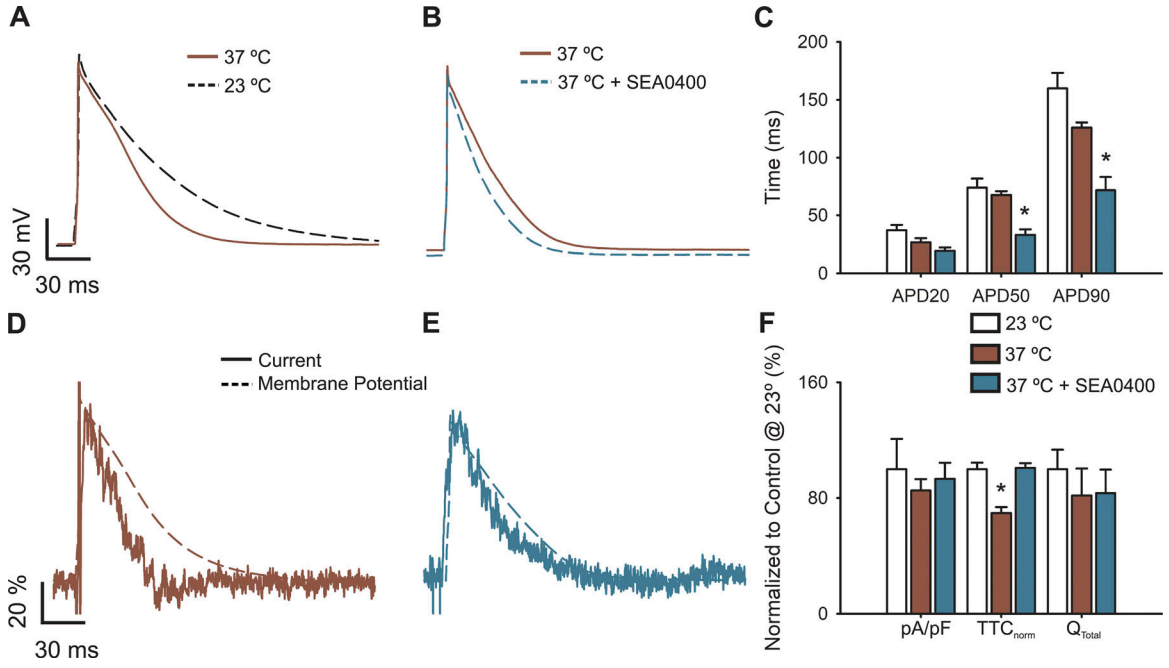

Figure 4. **Physiological temperature modifies APs and L-type calcium currents in cardiomyocytes. (A)** Representative AP waveforms from newborn rat cardiomyocytes at 23°–25°C (black dashed line) or 35°–37°C (brown line). **(B)** Representative AP waveforms at 35–37°C before (brown line) and after treatment with 1 µM SEA0400 (light blue line). APs were elicited by 2–5 ms depolarizing current injections (100–200 pA) at 1 Hz. **(C)** Bar graph of the APD percentage change upon isoproterenol treatment, estimated at 20% (APD_{20}), 50% (APD_{50}), and 90% (APD_{90}) of the repolarization phase. **(D and E)** Representative nifedipine-sensitive current (solid line) elicited by the AP (dashed line) prerecorded from the same cell at 35–37°C in control cardiomyocytes (D) or treated with 1 µM SEA0400 (E). **(F)** Bar graph of maximal current normalized by cell capacitance (pA/pF), total time of nifedipine-sensitive current normalized by its APD (TTC_{norm}), and the total current integral normalized by cell capacitance (Q_{total}). Data are presented as percentages with respect to control cardiomyocytes at 23–25°C. Bar graphs are mean ± SEM; empty bars represent control cardiomyocytes, brown bars correspond to cardiomyocytes at 35–37°C, and light blue bars correspond to cardiomyocytes at 35–37°C treated with 1 µM SEA0400. *, P < 0.01 with respect to control cardiomyocytes at 23–25°C.

The normalized current duration recorded in cardiomyocytes transfected with CaM_{34} did not differ from that of CaM_{wt}-overexpressing cardiomyocytes (Fig. 5 F), with both values approaching unity. Given the long duration of the current, the total mobilized charge was augmented (Fig. 5 F), indicating that, in the absence of CDI, total Ca^{2+} influx is increased. No changes in the maximal current were observed (−3.16 ± 0.52 and −3.05 ± 0.22 pA/pF for CaM_{wt} and CaM_{34}, respectively).

The contribution of VDI was evaluated by overexpressing the $Ca_V\beta_{2a}$ subunit, known to dramatically slow down VDI when overexpressed in cardiomyocytes (Moreno et al., 2015). For this set of data, cells infected with RFP were used as a control. $Ca_V\beta_{2a}$-transduced cardiomyocytes showed prolonged APs (400 ± 50 ms) with significant differences in all APDs measured (Fig. 6, A and B). Control RFP-transduced cardiomyocytes, however, showed APDs comparable to those of uninfected primary cells (137 ± 15 ms; Fig. 6 B). Furthermore, phase plots from these APs (Fig. 6 C) revealed changes in the overshoot (Fig. 6 D) and dV/dt_{max} (34.7 ± 9.8 and 74.3 ± 6.3 V/ms, respectively) when compared with RFP-overexpressing cardiomyocytes, likely as a result of increasing the number of channels at the plasma membrane (Moreno et al., 2015). Together, these results demonstrate that VDI is also instrumental in shaping the AP.

Nifedipine-sensitive current under sAP-Clamp configuration recorded from $Ca_V\beta_{2a}$-infected cardiomyocytes (Fig. 6 E) revealed similar TTC_{norm} when compared with RFP-transduced cardiomyocytes or controls, indicating that the current kinetics mirror those of their own elicited AP (Fig. 6 F). Nevertheless, the time to current peak was increased between RFP-transduced and $Ca_V\beta_{2a}$-infected cardiomyocytes (8.8 ± 0.2 to 26.2 ± 6.5 ms, respectively), and the L-type current amplitude became larger in VDI-impaired cardiomyocytes (RFP versus $Ca_V\beta_{2a}$: −3.82 ± 0.63 versus −5.40 ± 0.64 pA/pF; Fig. 6 F).

Next, we studied the effect of isoproterenol stimulation on the L-type calcium currents evoked under the sAP-Clamp configuration and found that, despite shortening of the APD (Fig. 1), β-adrenergic stimulation significantly affects the L-type calcium current. As a result, when both traces are normalized and overlaid, the L-type current does not follow the AP in isoproterenol-treated cells (Fig. 2 B). TTC_{norm} is 0.51 ± 0.07 in isoproterenol-stimulated cardiomyocytes, indicating that the AP is twice as slow as the nifedipine-sensitive current, whereas TTC_{norm} is 0.92 ± 0.03 in unstimulated cells, which reflects the similarities in the kinetics of both processes.

The present results suggest that at least one of the L-type channel inactivations may be promoted upon isoproterenol stimulus (Fig. 2 C shows the value of TTC_{norm} normalized by the TTC_{norm} in control conditions). Surprisingly, in sAP-Clamp recordings, neither the normalized peak L-type current (−3.79 ± 0.25 and −4.10 ± 0.49 for control and isoproterenol-treated cells, respectively) nor the total mobilized ionic charge differs between unstimulated and isoproterenol-treated cardiomyocytes

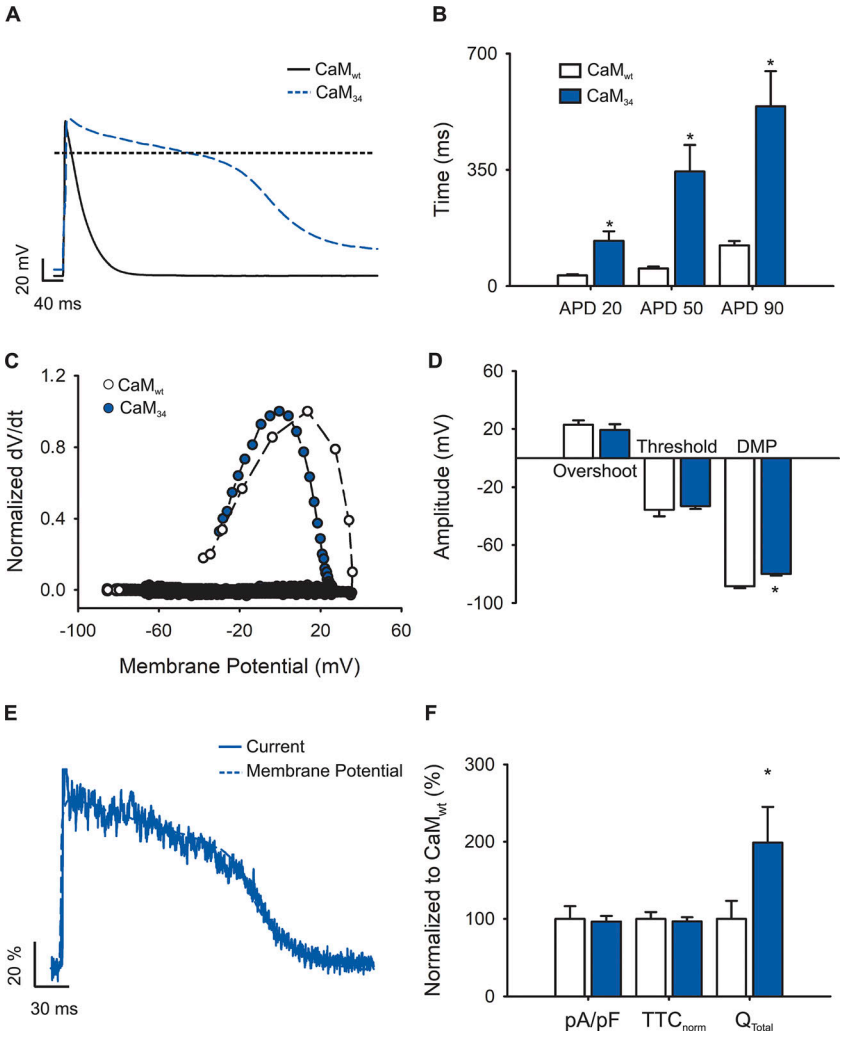

Figure 5. **APs and L-type calcium currents in CDI-impaired cardiomyocytes. (A)** Representative AP waveforms from a newborn rat cardiomyocyte overexpressing CaM_{wt} (solid black line) or CaM_{34} (dashed blue line). APs were elicited by 2–5 ms depolarizing current injections (100–200 pA) at 1 Hz. The horizontal line indicates zero level. **(B)** Bar graph of APD estimated at 20% (APD_{20}), 50% (APD_{50}), and 90% (APD_{90}) of the repolarization phase. **(C)** Phase plot of the normalized first derivative of membrane potential (dV/dt) against membrane potential (V_m) for the APs shown in A. Empty symbols correspond to data from cardiomyocytes overexpressing CaM_{wt} and blue symbols for cardiomyocytes overexpressing CaM_{34}. **(D)** Bar graph of overshoot, threshold potentials, and mean DMPs. **(E)** Representative nifedipine-sensitive current (solid line) elicited by the AP (dashed line) prerecorded from the same cardiomyocyte overexpressing CaM_{34}. **(F)** Bar graph of maximal current normalized by cell capacitance (pA/pF), total time of nifedipine-sensitive current normalized by its APD (TTC_{norm}), and the total current integral normalized by cell capacitance (Q_{total}). Data are shown as percentages with respect to CaM_{wt}-overexpressing cardiomyocytes. Bar graphs are mean ± SEM; empty bars represent cardiomyocytes overexpressing CaM_{wt} and blue bars correspond to those overexpressing CaM_{34} (n = 7; *, $P < 0.01$ with respect to CaM_{wt}).

(Fig. 2 C). The latter is in stark contrast with the behavior observed upon eliciting calcium currents with square pulses (Bers and Perez-Reyes, 1999; Kamp and Hell, 2000).

We infer that β-adrenergic stimulation not only increases L-type conductance but also could enhance inactivation with a concomitant reduction in current amplitude. In fact, doubling L-type maximal conductance in the mathematical model effectively augments the maximal current and the total mobilized charge; however, if boosting the maximal conductance is accompanied by more pronounced CDI or VDI, any change in peak current would be abrogated (Fig. 7 A). In the same line, the model predicts that if inactivation is not accentuated, β-adrenergic stimulation should heighten the maximal current.

To test this prediction and whether the diminished TTC_{norm} after β-adrenergic stimulation (Fig. 2) is dependent on the increase in a specific type of inactivation process, we compared the effects of impairing VDI or CDI in the current amplitude and kinetics upon β-adrenergic stimulation. As shown in Fig. 8, A and B, regardless of the inactivation type hindered, β-adrenergic stimulation resulted in faster AP repolarization. In fact, all APDs measured were significantly different between control and isoproterenol treatment in both $Ca_V\beta_{2a}$ (Fig. 8 A) and CaM_{34} (Fig. 8 B) -overexpressing cardiomyocytes. However, VDI-impaired cells showed more profound changes when compared with CDI-hindered cells, as demonstrated when the percentage of change after isoproterenol stimulation is compared (Fig. 8 C). Additionally, the phase plots in Fig. 8, D and E, expose changes in overshoot without alterations in the DMP or the threshold potential (Fig. 8 F).

Interestingly, evaluation of the nifedipine-sensitive current under sAP-Clamp configuration in VDI-deficient cardiomyocytes stimulated with isoproterenol (Fig. 9 B) indicated that, as in control RFP-transduced cells (Fig. 9 A), the current kinetics does not follow the AP kinetics with a TTC_{norm} of 0.61 ± 0.03 (Fig. 9 C for values normalized with respect to RFP-transduced cardiomyocytes).In contrast, this current parallels the AP in cardiomyocytes overexpressing CaM_{34} that were stimulated with isoproterenol (Fig. 9 E) with a TTC_{norm} of 0.95 ± 0.02 (Fig. 9 F for values normalized with respect to CaM_{wt}-overexpressing cardiomyocytes). Expectedly, the current kinetics does not match the AP in cardiomyocytes overexpressing CaM_{wt} (Fig. 9 D).

Isoproterenol treatment did not detectably change any of the parameters quantified (peak current, time to peak, or total mobilized charge) in $Ca_V\beta_{2a}$-overexpressing cardiomyocytes (Figs. 7 B and 9 C). In contrast, cardiomyocytes overexpressing

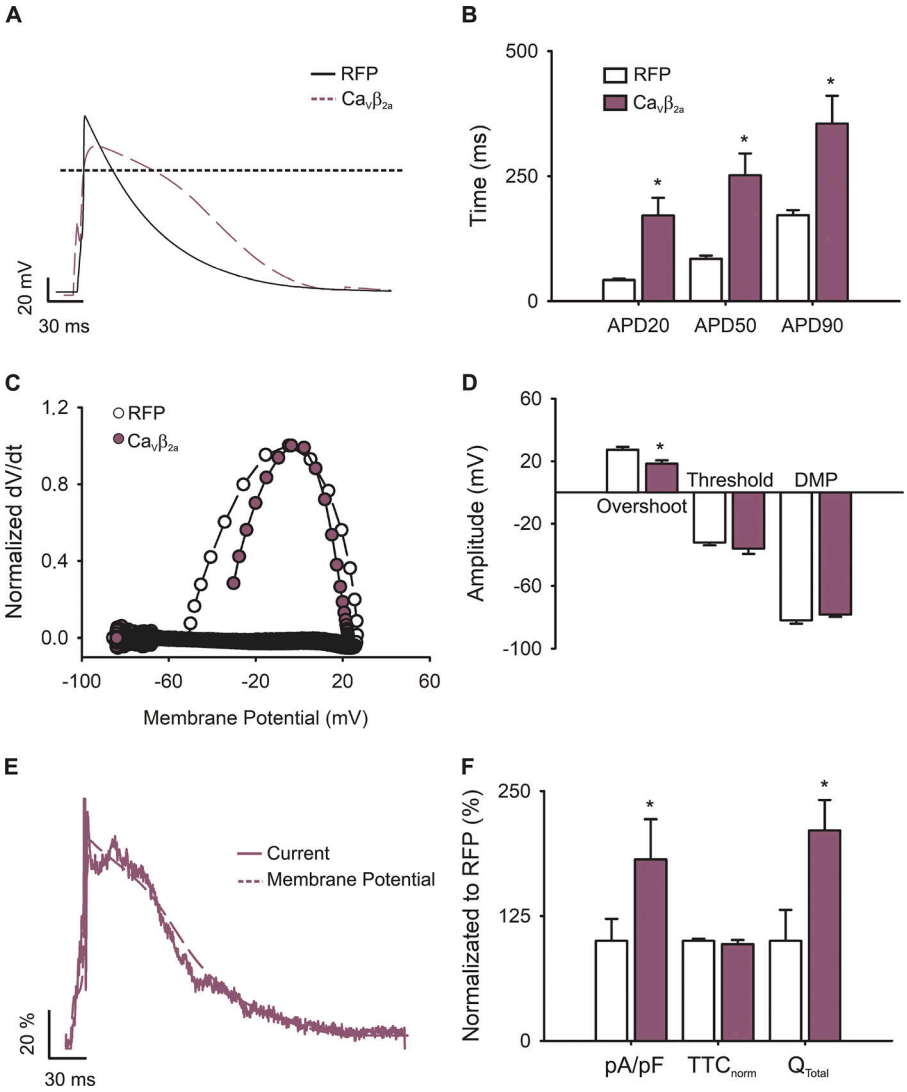

Figure 6. **APs and L-type calcium currents in VDI-impaired newborn rat cardiomyocytes. (A)** Representative AP waveforms from a newborn rat cardiomyocyte overexpressing RFP (solid black line) or Ca$_V\beta_{2a}$ (dashed plum line). APs were elicited by 2–5 ms depolarizing current injections (100–200 pA) at 1 Hz. **(B)** Bar graph of APD estimated at 20% (APD$_{20}$), 50% (APD$_{50}$), and 90% (APD$_{90}$) of the repolarization phase. **(C)** Phase plot of the normalized first derivative of membrane potential (dV/dt) against membrane potential (V$_m$) for the APs shown in A. Cardiomyocytes overexpressing RFP are shown with empty symbols and cardiomyocytes overexpressing Ca$_V\beta_{2a}$ with plum symbols. **(D)** Bar graph of overshoot, threshold potentials, and mean DMPs. **(E)** Representative nifedipine-sensitive current (solid line) elicited by the AP (dashed line) prerecorded from the same cardiomyocyte overexpressing Ca$_V\beta_{2a}$. **(F)** Bar graph of maximal current normalized by cell capacitance (pA/pF), total time of nifedipine-sensitive current normalized by its APD (TTC$_{norm}$), and the total current integral normalized by cell capacitance (Q$_{total}$). Data are presented as percentages with respect to RFP-transduced cardiomyocytes. Bar graphs are mean ± SEM; empty bars represent cardiomyocytes overexpressing RFP, and plum bars correspond to those overexpressing Ca$_V\beta_{2a}$ (n = 6; *, P < 0.01 with respect to RFP).

CaM$_{34}$ exhibited higher peak currents upon β-adrenergic stimulation, with clear changes in total mobilized charge observed in the CaM mutant compared with CaM$_{wt}$ cells (Figs. 7 B and 9 F). These results demonstrate that CDI, and not VDI, is the predominant inactivation process during β-adrenergic stimulation.

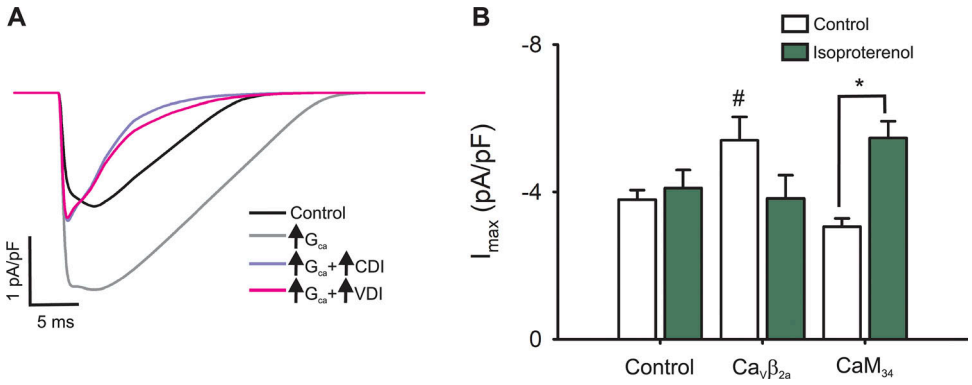

Figure 7. **Role of L-type channel inactivation processes during a simulated AP. (A)** Simulated L-type calcium current for the control condition (black line) or for cardiomyocytes with increased L-type channel conductance alone (light gray line) or simultaneously with an increased CDI (violet line) or VDI (pink line). **(B)** Experimental data showing the maximal nifedipine-sensitive current from control, Ca$_V\beta_{2a}$, and CaM$_{34}$ before (empty bars) or after (green bars) isoproterenol stimulation. #, P < 0.01 with respect to control; *, P < 0.01 between values before and after isoproterenol stimulation.

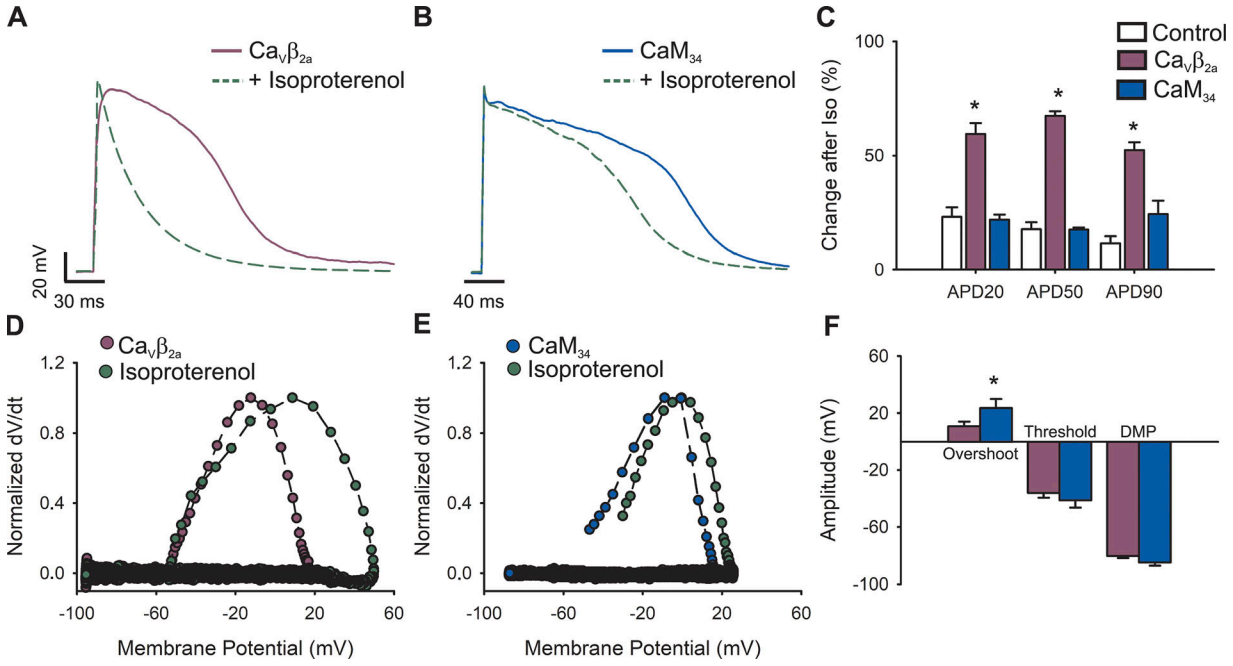

Figure 8. **Role of VDI and CDI on APs upon β-adrenergic stimulus. (A and B)** Representative AP waveforms from newborn rat cardiomyocytes overexpressing $Ca_V\beta_{2a}$ (A) or CaM_{34} (B) before (solid lines) and after (dashed green lines) stimulus with 100 nM isoproterenol. APs were elicited by 2–5 ms depolarizing current injections (100–200 pA) at 1 Hz. **(C)** Bar graph of the APD percentage change upon isoproterenol treatment, estimated at 20% (APD_{20}), 50% (APD_{50}), and 90% (APD_{90}) of the repolarization phase. **(D and E)** Phase plots of the normalized first derivative of membrane potential (dV/dt) against membrane potential (V_m) for the APs shown in A and B, respectively. Plum symbols correspond to $Ca_V\beta_{2a}$-overexpressing cardiomyocytes, blue symbols to CaM_{34}-overexpressing cardiomyocytes, and green symbols to the isoproterenol-treated condition. **(F)** Bar graph of overshoot, threshold potentials, and mean DMPs from cardiomyocytes treated with isoproterenol and overexpressing $Ca_V\beta_{2a}$ or CaM_{34}. Bar graphs are mean ± SEM. *, $P < 0.01$, with respect to control.

Discussion

The individual contribution of VDI and CDI in the regulation of the L-type calcium current during an AP is an open question. Diverse kinetic models have predicted that both inactivation processes are important in shaping L-type current kinetics during the cardiac AP because impairment of either type of inactivation leads to an increase in APD; however, the relative contribution of each process is still debated (Findlay, 2004; Morotti et al., 2012; Kumari et al., 2018). In this study, we combined the use of sAP-Clamp with the overexpression of specific proteins that impair either VDI or CDI to assess their contribution to the L-type current kinetics in primary newborn rat cardiomyocytes. We also implemented a mathematical model (Wang and Sobie, 2008) that provided support and predictions aimed at testing the different hypotheses. The use of sAP-Clamp allowed us to directly compare the kinetics of the endogenous L-type current during its own AP. Thus, the specific post-translational modifications that could modify the inactivation kinetics on each cell are accounted for under this configuration, in contrast with experiments performed using standardized (or prerecorded) AP waveforms.

At the molecular level, CDI requires the binding of Ca^{2+} to CaM, which is constitutively tethered to a region of the $Ca_V1.2$ C-terminus (the IQ domain). The source of Ca^{2+} for initiating CDI could be either the Ca^{2+} entering the cell through the L-type channels or released from the sarcoplasmic reticulum, with the latter source controlling CDI during the initial AP phase and the former modulating the remaining of the AP (Morotti et al., 2012). However, considering the experimental condition used in this study and the fact that newborn cardiomyocytes present immature T-tubules, the main Ca^{2+} source for CDI expected here is the influx of calcium through the L-type channels. The demonstration that NCX activity, in our experimental control conditions, does not shape the AP (Fig. S4) suggests that the cardiomyocytes from newborn rats represent a particular model of study, in which the LTCC activity is weakly modulated by changes in intracellular calcium concentration.

Thus, although the observation that nifedipine-sensitive current kinetics mirror the AP is hardly extrapolated to other models with higher NCX activity or with fully developed dyads, the relevance of each inactivation process during the AP demonstrated here and the dominance of CDI upon β-adrenergic stimulation are likely valid in cardiomyocytes where the L-type current CDI is pronounced, as in the case of adult cardiomyocytes, an observation supported by the mathematical model (Figs. 3 and 7).

Previous investigations have replaced external Ca^{2+} by other charge carriers in order to eliminate CDI and isolate the VDI contribution (Hadley and Hume, 1987; Yuan et al., 1996; Findlay, 2002; Morad and Soldatov, 2005). However, these maneuvers overestimate VDI, because some degree of inactivation dependent on the permeable ion is still observed (Brunet et al., 2009; Grandi et al., 2010). Here we used the molecular approach of overexpressing a mutant version of CaM (CaM_{34}) known to abolish CDI (Alseikhan et al., 2002) and facilitate the study of L-type current with predominantly VDI during AP firing.

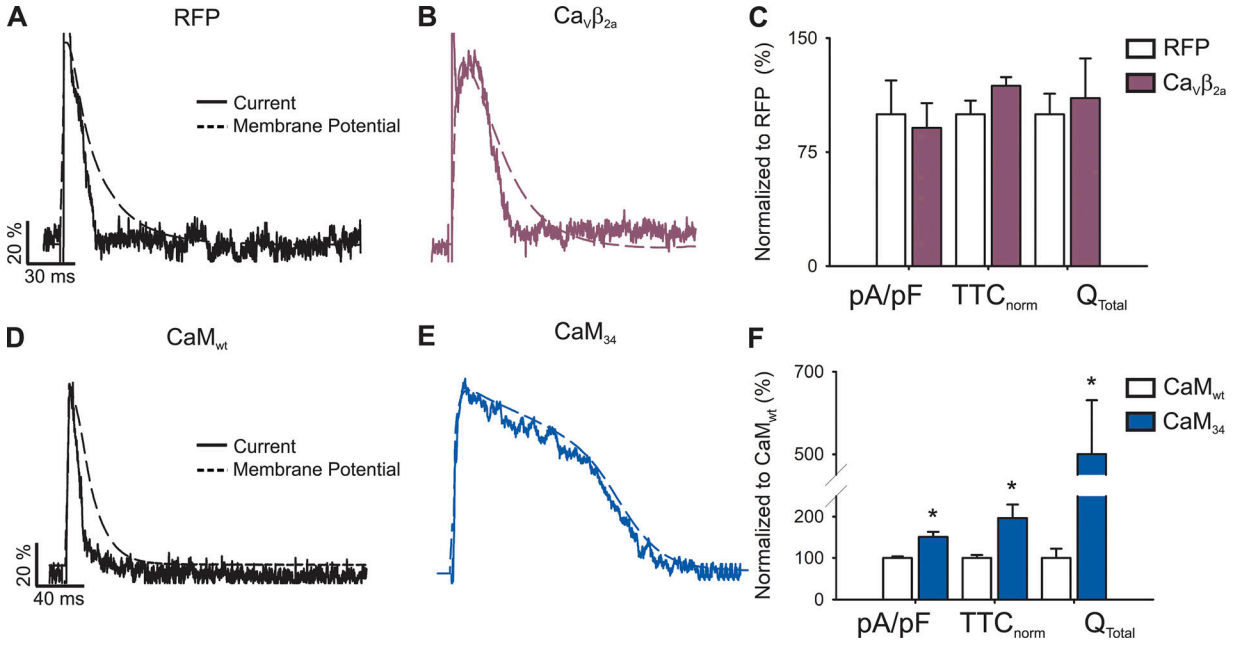

Figure 9. **L-type channel inactivation processes upon β-adrenergic stimulus.** Representative nifedipine-sensitive current (solid line) elicited by the AP (dashed line) prerecorded from the same cell in a newborn rat cardiomyocyte overexpressing RFP (A), $Ca_V\beta_{2a}$ (B), CaM_{wt} (D), or CaM_{34} (E). Bar graphs are mean ± SEM (n = 8) of maximal current normalized by cell capacitance (pA/pF), total time of current normalized by action potential duration (TTC_{norm}), and the total current integral normalized by cell capacitance (Q_{total}) from a cardiomyocyte overexpressing RFP (empty bars) and $Ca_V\beta_{2a}$ (plum bars). CaM_{wt} (empty bars; B) or CaM_{34} (blue bars; D). Data are presented as percentages of their respective control situation [RFP for C and CaM_{wt} for F]. *, P < 0.01 with respect to control.

Conversely, the G406R mutation linked to Timothy syndrome (Faber et al., 2007) has been shown to reduce VDI (Splawski et al., 2004), thus isolating CDI. However, this mutation causes apparent changes in the activation kinetics of the current (Yarotskyy et al., 2009); in addition, recent work has shown that the CDI is also affected with this mutation (Dick et al., 2016), which implies inaccuracy in any relative estimation of either inactivation process. In this work we overexpressed the $Ca_V\beta_{2a}$ subunit, known to impair the VDI of the L-type current when overexpressed in cardiomyocytes (Moreno et al., 2015). Although overexpression of this auxiliary subunit does not completely abolish VDI, CDI should not be affected, and thus the L-type current kinetics under this condition would be dominated by CDI.

The overexpression of either molecule is not without unwanted consequences, because the $Ca_V\beta_{2a}$ subunit affects other L-type channel processes, such as activation kinetics and the total amount of channels at the plasma membrane (Moreno et al., 2015). This explains the observed changes in overshoot, maximal depolarization velocity, and peak current at the beginning of the AP, as well as the slow time to peak recorded in the nifedipine-sensitive current and AP from $Ca_V\beta_{2a}$-overexpressing cardiomyocytes (Fig. 6). In turn, overexpression of CaM_{34} can potentially modify other CaM-dependent ion channels, such as voltage-dependent sodium channels (Yan et al., 2017). This may explain a mildly depolarized phenotype observed in cardiomyocytes overexpressing this mutant form of CaM (Fig. 5). Nevertheless, both molecular tools, CaM_{34} and $Ca_V\beta_{2a}$, are specific to each inactivation process (CDI and VDI, respectively), allowing us to regulate independently each inactivation process.

The impairment of either VDI or CDI induces AP prolongation (Figs. 3, 5, and 6), indicating that both inactivation types shape L-type current kinetics during the cardiac AP. However, a closer look at the kinetics revealed that the main difference between both conditions resides at the intermediate phase of the AP, as the difference between APD_{50} and APD_{20} (ΔAPD_{50-20}) in CaM_{34}-overexpressing cardiomyocytes is almost three times higher than that of $Ca_V\beta_{2a}$-overexpressing cardiomyocytes (221 ± 80 versus 70 ± 14 ms). Remarkably, in cardiomyocytes where VDI and CDI are simultaneously impaired (by coexpression of $Ca_V\beta_{2a}$ and CaM_{34}) APD_{20} is greater than in cardiomyocytes with either one of the inactivation processes affected (Fig. S5), suggesting than both inactivation processes can independently modulate the L-type current during the initial phase of the AP.

Our results demonstrate that, under control conditions, CDI and VDI are important in the initial AP phase, while CDI dominates at later times. Interestingly, the L-type current mirrors the kinetics of the AP in control cardiomyocytes and those where either inactivation has been hindered (Figs. 2, 5, and 6). This highlights the importance of the transition between open and closed channels (deactivation) in the control of the L-type calcium current. This seems particularly significant during latter parts of the AP, where the potassium channels are activated, and was recapitulated by the mathematical model (Fig. 3).

In isoproterenol-stimulated cardiomyocytes, the calcium current no longer matches the kinetics of the AP (Fig. 2),

indicating that at least one of the inactivation processes becomes more preponderant. Because this effect remains when VDI is compromised, but not when CDI is abolished (Fig. 9), it is reasonable to conclude that the calcium-dependent inactivation process predominates under β-adrenergic stimulation. Repolarization depends on potassium and calcium permeability; thus, the augmented effect of isoproterenol on VDI-impaired cardiomyocyte APs compared with CDI-deficient or control cardiomyocytes (Fig. 8) strongly suggests that β-adrenergic stimulation indeed suppresses the VDI process in cardiomyocytes.

Under β-adrenergic stimulus, square pulse protocols have shown up to threefold increases in peak L-type current (Miriyala et al., 2008). In contrast, stimulation via a more physiological waveform using sAP-Clamp failed to display augmented L-type currents in isoproterenol-treated cells, albeit faster inactivation kinetics were observed, indicating that the total ionic charge transferred during the AP is actually reduced (Fig. 2).

These results are adequately recapitulated by the mathematical model, showing that a simultaneous increase in maximal conductance and the relative contribution of inactivation leads to L-type currents with essentially the same peak current and mobilizing charge (Fig. 7 A). Our experimental observation of enhanced peak currents only in isoproterenol-treated CDI-deficient cardiomyocytes and not in those that are VDI-deficient (Fig. 7 B) shows the role of each inactivation process in L-type current control upon β-adrenergic stimulation.

In summary, with this molecular approach, we demonstrate that, under β-adrenergic stimulation, CDI is increased, whereas VDI is reduced. As a result of these modifications and their effect on inactivation kinetics, the total duration of the current is diminished and therefore less calcium enters the cell during one AP.

The maintaining of the plateau phase of the AP in the absence of the L-type current upon β-adrenergic stimulus (Fig. 2) could be explained by NCX-dependent depolarization permeability. Whether the activity of this exchanger is modified upon β-adrenergic stimulation in newborn rat cardiomyocytes, as has been proved in other species (Perchenet et al., 2000), remains unknown. However, in order to maintain calcium homeostasis, calcium entering the cell through L-type channels must be extruded by the NCX exchanger; therefore, our results seem to preclude major β-adrenergic modulation of NCX activity.

These conclusions also imply that the well-established increase in the calcium transient amplitude after a β-adrenergic stimulus in newborn rat cardiomyocytes is likely a consequence of ryanodine receptor modification, accompanied by a concomitant increase in SERCA activity, and not a consequence of LTCC modification. Whether this occurs in cardiomyocytes with higher L-type current and stronger CDI due to the coupling between L-type Ca^{2+} channels and ryanodine receptors, such as adult cardiomyocytes, remains to be demonstrated.

Acknowledgments

We thank Dr. Rocio K. Finol-Urdaneta and Dr. Jeffrey R. McArthur (Illawarra Health and Medical Research Institute, University of Wollongong) for constructive discussion of the work and Dr. Eric Sobie for sharing the code used for modeling the L-type current.

This work was supported by a research grant from Fondo Nacional de Desarrollo Científico y Tecnológico (Fondecyt; grant 1160900 to D. Varela). The Millennium Nucleus of Ion Channels-Associated Diseases (MiNICAD) is a Millennium Nucleus supported by the Iniciativa Científica Milenio of the Ministry of Economy, Development and Tourism (Chile).

The authors declare no competing financial interests.

Author contributions: D. Morales and D. Varela designed the project. D. Morales performed the experiments. D. Morales, T. Hermosilla, and D. Varela analyzed the data. D. Varela and T. Hermosilla wrote the manuscript.

Eduardo Ríos served as editor.

Submitted: 6 September 2018
Accepted: 10 February 2019

References

Alseikhan, B.A., C.D. DeMaria, H.M. Colecraft, and D.T. Yue. 2002. Engineered calmodulins reveal the unexpected eminence of Ca2+ channel inactivation in controlling heart excitation. *Proc. Natl. Acad. Sci. USA.* 99: 17185–17190. https://doi.org/10.1073/pnas.262372999

Armoundas, A.A., I.A. Hobai, G.F. Tomaselli, R.L. Winslow, and B. O'Rourke. 2003. Role of sodium-calcium exchanger in modulating the action potential of ventricular myocytes from normal and failing hearts. *Circ. Res.* 93:46–53. https://doi.org/10.1161/01.RES.0000080932.98903.D8

Benitah, J.P., J.L. Alvarez, and A.M. Gómez. 2010. L-type Ca(2+) current in ventricular cardiomyocytes. *J. Mol. Cell. Cardiol.* 48:26–36. https://doi.org/10.1016/j.yjmcc.2009.07.026

Bers, D.M., and E. Perez-Reyes. 1999. Ca channels in cardiac myocytes: structure and function in Ca influx and intracellular Ca release. *Cardiovasc. Res.* 42:339–360. https://doi.org/10.1016/S0008-6363(99)00038-3

Bondarenko, V.E., G.P. Szigeti, G.C. Bett, S.J. Kim, and R.L. Rasmusson. 2004. Computer model of action potential of mouse ventricular myocytes. *Am. J. Physiol. Heart Circ. Physiol.* 287:H1378–H1403. https://doi.org/10.1152/ajpheart.00185.2003

Brunet, S., T. Scheuer, and W.A. Catterall. 2009. Cooperative regulation of Ca(v)1.2 channels by intracellular Mg(2+), the proximal C-terminal EF-hand, and the distal C-terminal domain. *J. Gen. Physiol.* 134:81–94. https://doi.org/10.1085/jgp.200910209

Bünemann, M., B.L. Gerhardstein, T. Gao, and M.M. Hosey. 1999. Functional regulation of L-type calcium channels via protein kinase A-mediated phosphorylation of the beta(2) subunit. *J. Biol. Chem.* 274:33851–33854. https://doi.org/10.1074/jbc.274.48.33851

Dick, I.E., R. Joshi-Mukherjee, W. Yang, and D.T. Yue. 2016. Arrhythmogenesis in Timothy syndrome is associated with defects in Ca(2+)-dependent inactivation. *Nat. Commun.* 7:10370. https://doi.org/10.1038/ncomms10370

Faber, G.M., J. Silva, L. Livshitz, and Y. Rudy. 2007. Kinetic properties of the cardiac L-type Ca2+ channel and its role in myocyte electrophysiology: a theoretical investigation. *Biophys. J.* 92:1522–1543. https://doi.org/10.1529/biophysj.106.088807

Fabiato, A. 1983. Calcium-induced release of calcium from the cardiac sarcoplasmic reticulum. *Am. J. Physiol.* 245:C1–C14. https://doi.org/10.1152/ajpcell.1983.245.1.C1

Findlay, I. 2002. Voltage- and cation-dependent inactivation of L-type Ca2+ channel currents in guinea-pig ventricular myocytes. *J. Physiol.* 541: 731–740. https://doi.org/10.1113/jphysiol.2002.019729

Findlay, I. 2004. Physiological modulation of inactivation in L-type Ca2+ channels: one switch. *J. Physiol.* 554:275–283. https://doi.org/10.1113/jphysiol.2003.047902

Fuller, M.D., M.A. Emrick, M. Sadilek, T. Scheuer, and W.A. Catterall. 2010. Molecular mechanism of calcium channel regulation in the fight-or-flight response. *Sci. Signal.* 3:ra70. https://doi.org/10.1126/scisignal.2001152

Grandi, E., S. Morotti, K.S. Ginsburg, S. Severi, and D.M. Bers. 2010. Interplay of voltage and Ca-dependent inactivation of L-type Ca current. *Prog.*

Biophys. Mol. Biol. 103:44–50. https://doi.org/10.1016/j.pbiomolbio.2010.02.001

Haase, H., S. Bartel, P. Karczewski, I. Morano, and E.G. Krause. 1996. In-vivo phosphorylation of the cardiac L-type calcium channel beta-subunit in response to catecholamines. *Mol. Cell. Biochem.* 163-164:99–106. https://doi.org/10.1007/BF00408645

Hadley, R.W., and J.R. Hume. 1987. An intrinsic potential-dependent inactivation mechanism associated with calcium channels in guinea-pig myocytes. *J. Physiol.* 389:205–222. https://doi.org/10.1113/jphysiol.1987.sp016654

Hamill, O.P., A. Marty, E. Neher, B. Sakmann, and F.J. Sigworth. 1981. Improved patch-clamp techniques for high-resolution current recording from cells and cell-free membrane patches. *Pflugers Arch.* 391:85–100. https://doi.org/10.1007/BF00656997

Hermosilla, T., C. Moreno, M. Itfinca, C. Altier, R. Armisén, A. Stutzin, G.W. Zamponi, and D. Varela. 2011. L-type calcium channel β subunit modulates angiotensin II responses in cardiomyocytes. *Channels (Austin).* 5:280–286. https://doi.org/10.4161/chan.5.3.15833

Hermosilla, T., M. Encina, D. Morales, C. Moreno, C. Conejeros, H.M. Alfaro-Valdés, F. Lagos-Meza, F. Simon, C. Altier, and D. Varela. 2017. Prolonged AT_1R activation induces $Ca_V1.2$ channel internalization in rat cardiomyocytes. *Sci. Rep.* 7:10131. https://doi.org/10.1038/s41598-017-10474-z

Hulme, J.T., R.E. Westenbroek, T. Scheuer, and W.A. Catterall. 2006. Phosphorylation of serine 1928 in the distal C-terminal domain of cardiac CaV1.2 channels during beta1-adrenergic regulation. *Proc. Natl. Acad. Sci. USA.* 103:16574–16579. https://doi.org/10.1073/pnas.0607294103

Kääb, S., H.B. Nuss, N. Chiamvimonvat, B. O'Rourke, P.H. Pak, D.A. Kass, E. Marban, and G.F. Tomaselli. 1996. Ionic mechanism of action potential prolongation in ventricular myocytes from dogs with pacing-induced heart failure. *Circ. Res.* 78:262–273. https://doi.org/10.1161/01.RES.78.2.262

Kamp, T.J., and J.W. Hell. 2000. Regulation of cardiac L-type calcium channels by protein kinase A and protein kinase C. *Circ. Res.* 87:1095–1102. https://doi.org/10.1161/01.RES.87.12.1095

Katchman, A., L. Yang, S.I. Zakharov, J. Kushner, J. Abrams, B.X. Chen, G. Liu, G.S. Pitt, H.M. Colecraft, and S.O. Marx. 2017. Proteolytic cleavage and PKA phosphorylation of α_{1C} subunit are not required for adrenergic regulation of $Ca_V1.2$ in the heart. *Proc. Natl. Acad. Sci. USA.* 114:9194–9199. https://doi.org/10.1073/pnas.1706054114

Kumari, N., H. Gaur, and A. Bhargava. 2018. Cardiac voltage gated calcium channels and their regulation by ββ-adrenergic signaling. *Life Sci.* 194:139–149. https://doi.org/10.1016/j.lfs.2017.12.033

Marks, A.R. 2013. Calcium cycling proteins and heart failure: mechanisms and therapeutics. *J. Clin. Invest.* 123:46–52. https://doi.org/10.1172/JCI62834

Miriyala, J., T. Nguyen, D.T. Yue, and H.M. Colecraft. 2008. Role of CaVbeta subunits, and lack of functional reserve, in protein kinase A modulation of cardiac CaV1.2 channels. *Circ. Res.* 102:e54–e64. https://doi.org/10.1161/CIRCRESAHA.108.171736

Morad, M., and N. Soldatov. 2005. Calcium channel inactivation: possible role in signal transduction and Ca2+ signaling. *Cell Calcium.* 38:223–231. https://doi.org/10.1016/j.ceca.2005.06.027

Moreno, C., T. Hermosilla, D. Morales, M. Encina, L. Torres-Díaz, P. Díaz, D. Sarmiento, F. Simon, and D. Varela. 2015. Cavβ2 transcription start site variants modulate calcium handling in newborn rat cardiomyocytes. *Pflugers Arch.* 467:2473–2484. https://doi.org/10.1007/s00424-015-1723-3

Morotti, S., E. Grandi, A. Summa, K.S. Ginsburg, and D.M. Bers. 2012. Theoretical study of L-type Ca(2+) current inactivation kinetics during action potential repolarization and early afterdepolarizations. *J. Physiol.* 590:4465–4481. https://doi.org/10.1113/jphysiol.2012.231886

O'Hara, T., and Y. Rudy. 2012. Quantitative comparison of cardiac ventricular myocyte electrophysiology and response to drugs in human and non-human species. *Am. J. Physiol. Heart Circ. Physiol.* 302:H1023–H1030. https://doi.org/10.1152/ajpheart.00785.2011

Perchenet, L., A.K. Hinde, K.C. Patel, J.C. Hancox, and A.J. Levi. 2000. Stimulation of Na/Ca exchange by the beta-adrenergic/protein kinase A pathway in guinea-pig ventricular myocytes at 37 degrees C. *Pflugers Arch.* 439:822–828.

Peterson, B.Z., C.D. DeMaria, J.P. Adelman, and D.T. Yue. 1999. Calmodulin is the Ca2+ sensor for Ca2+ -dependent inactivation of L-type calcium channels. *Neuron.* 22:549–558. https://doi.org/10.1016/S0896-6273(00)80709-6

Ramos-Franco, J., Y. Aguilar-Sanchez, and A.L. Escobar. 2016. Intact heart loose patch photolysis reveals ionic current kinetics during ventricular action potentials. *Circ. Res.* 118:203–215. https://doi.org/10.1161/CIRCRESAHA.115.307399

Song, Y., J.C. Shryock, H.J. Knot, and L. Belardinelli. 2001. Selective attenuation by adenosine of arrhythmogenic action of isoproterenol on ventricular myocytes. *Am. J. Physiol. Heart Circ. Physiol.* 280:H2789–H2795. https://doi.org/10.1152/ajpheart.2001.280.6.H2789

Splawski, I., K.W. Timothy, L.M. Sharpe, N. Decher, P. Kumar, R. Bloise, C. Napolitano, P.J. Schwartz, R.M. Joseph, K. Condouris, et al. 2004. Ca(V)1.2 calcium channel dysfunction causes a multisystem disorder including arrhythmia and autism. *Cell.* 119:19–31. https://doi.org/10.1016/j.cell.2004.09.011

Tsien, R.W., B.P. Bean, P. Hess, J.B. Lansman, B. Nilius, and M.C. Nowycky. 1986. Mechanisms of calcium channel modulation by beta-adrenergic agents and dihydropyridine calcium agonists. *J. Mol. Cell. Cardiol.* 18:691–710. https://doi.org/10.1016/S0022-2828(86)80941-5

Wang, L.J., and E.A. Sobie. 2008. Mathematical model of the neonatal mouse ventricular action potential. *Am. J. Physiol. Heart Circ. Physiol.* 294:H2565–H2575. https://doi.org/10.1152/ajpheart.01376.2007

Weiss, S., S. Oz, A. Benmocha, and N. Dascal. 2013. Regulation of cardiac L-type Ca^{2+} channel CaV1.2 via the β-adrenergic-cAMP-protein kinase A pathway: old dogmas, advances, and new uncertainties. *Circ. Res.* 113:617–631. https://doi.org/10.1161/CIRCRESAHA.113.301781

Woo, A.Y., and R.P. Xiao. 2012. ββ-Adrenergic receptor subtype signaling in heart: from bench to bedside. *Acta Pharmacol. Sin.* 33:335–341. https://doi.org/10.1038/aps.2011.201

Xu, H., M. Zhao, S. Liang, Q. Huang, Y. Xiao, L. Ye, Q. Wang, L. He, L. Ma, H. Zhang, et al. 2016. The effects of puerarin on rat ventricular myocytes and the potential mechanism. *Sci. Rep.* 6:35475. https://doi.org/10.1038/srep35475

Yan, H., C. Wang, S.O. Marx, and G.S. Pitt. 2017. Calmodulin limits pathogenic Na+ channel persistent current. *J. Gen. Physiol.* 149:277–293. https://doi.org/10.1085/jgp.201611721

Yarotskyy, V., G. Gao, B.Z. Peterson, and K.S. Elmslie. 2009. The Timothy syndrome mutation of cardiac CaV1.2 (L-type) channels: multiple altered gating mechanisms and pharmacological restoration of inactivation. *J. Physiol.* 587:551–565. https://doi.org/10.1113/jphysiol.2008.161737

Yuan, W., K.S. Ginsburg, and D.M. Bers. 1996. Comparison of sarcolemmal calcium channel current in rabbit and rat ventricular myocytes. *J. Physiol.* 493:733–746. https://doi.org/10.1113/jphysiol.1996.sp021418

Yue, D.T., S. Herzig, and E. Marban. 1990. Beta-adrenergic stimulation of calcium channels occurs by potentiation of high-activity gating modes. *Proc. Natl. Acad. Sci. USA.* 87:753–757. https://doi.org/10.1073/pnas.87.2.753